

Ink-jet Printing of High-Molecular-Weight Polymers in Oil-in-Water Emulsions

*Ashley S. Johns and Colin D. Bain**

Department of Chemistry, Durham University, South Road, Durham, DH1 3LE, United
Kingdom

KEYWORDS

Ink-jet printing, polymers, non-Newtonian fluids, viscoelasticity, emulsions

ABSTRACT

Ink-jet printing of high-molecular-weight polymers is inhibited by the extensional elasticity of the polymer chains. This paper describes how emulsions can be used to print high-molecular-weight polymers at much higher concentrations than is possible in a binary solution. The polymers are dissolved in the dispersed phase of an oil-in-water emulsion. The surface tension of the oil-water interface opposes deformation of the oil droplets during ejection from the nozzle and leads to the extensional strain occurring in the polymer-free continuous phase. We show that a solution of polystyrene ($M_n = 419$ kDa, polydispersity index = 1.21) can be printed at an overall concentration of 3.8 %wt in an SDS-stabilized emulsion of methyl benzoate in water, an order of magnitude higher in concentration than previously reported for polystyrene dissolved in binary solutions [Hoath, S. D.; Harlen, O. G.; Hutchings, I. M. *J. Rheol.* **2012**, *56* (5), 1109–

1127]. Factors influencing the formulation of emulsions for ink-jet printing of polymers are discussed.

INTRODUCTION

Ink-jet printing technology has developed since the 1960s and 1970s into a familiar and commonplace technique.¹⁻³ The best-established applications are in product marking and digital graphics. Ink-jet technology allows small volumes of fluid to be delivered to a substrate in a controlled and repeatable manner so that high-resolution arrays can be constructed from a digital file. The strengths of ink-jet printing mean that it is suitable for a wealth of applications beyond the deposition of inks and pigments.^{4,5} Ink-jet technology has been used, for example, to build three-dimensional structures using ceramic inks⁶ and print conductive silver tracks.⁷ The technology has also been used to deposit functional polymers during the manufacture of organic solar cells^{8,9} and organic light-emitting diode displays.¹⁰ Studies have shown that control over deposit morphology and advanced patterning of substrates can be achieved using careful formulation design.¹¹

As the range of applications of ink-jet technology grows, so does the complexity of the inks. Polymers are frequently included in ink-jet formulations at low concentrations to optimize the viscosity for ink-jet printing⁴ and to confer greater stability upon pigment dispersions.¹² They can also improve printing behavior by reducing satellite production and thus improve pattern resolution.^{13,14} At increased concentration, however, it becomes impractical to jet polymer solutions because non-Newtonian effects have a dramatic impact upon the ejection of a drop from the nozzle. A Newtonian liquid necks under capillary pressure to a pinch point, after which the drop detaches.¹⁵ Polymer solutions initially follow these dynamics¹⁶ but, on the approach to

the pinch point, the fluid experiences very high strain rates, σ , that trigger the sudden generation of a thin, cylindrical filament between the main drop and the orifice.¹⁵ Filament formation is caused by the polymer chains undergoing a coil-stretch transition, which for a linear polymer is expected when $\sigma > (2\tau)^{-1}$, where τ is the longest polymer relaxation time.¹⁷ The radius of the filament no longer decreases according to Newtonian dynamics, but instead decays exponentially so that drop breakoff time is significantly increased.¹⁶ The importance of polymer relaxation dynamics in governing the thinning of the filament increases strongly with increasing polymer concentration and molecular weight.¹⁸ The eventual rupture of the filament can lead to the production of satellites, particularly if the filament takes on a “beads-on-a-string” structure prior to breakoff.¹⁹ The coil-stretch transition also decelerates the main drop as a result of the increase in elasticity to the extent that the drop may fail to detach at all and be drawn back into the residual fluid in the orifice.²⁰ The non-Newtonian behavior of polymer solutions therefore places practical limits on the concentration of a printable polymer solution. For example, Hoath *et al.*²¹ reported that the maximum printable concentration of a polystyrene (PS) solution in diethyl phthalate (DEP) with a molecular weight of 488 kDa was of the order 0.25 %wt. It is possible to manufacture and print highly-loaded formulations if the polymer is present as a solid, as demonstrated with low-MW polyurethane colloidal suspensions with a 40-%wt solids content.²²

In this paper, we show that oil-in-water emulsions can be used to overcome the limitations of printing high-molecular-weight polymers in solution. The polymer is dissolved in a good solvent and dispersed as the discontinuous phase of an emulsion, with a surfactant as a stabilizer. The emulsion droplets shield the polymers from the high strain rates that cause them to undergo the coil-stretch transition and thus allow them to be printed at a higher overall concentration. The

underlying physical mechanism is the resistance to deformation provided by the free energy, G , of the oil-water interface. The interfacial free energy can be simply expressed as

$$G = \gamma A, \quad (1)$$

where γ is the interfacial tension and A is the area of the interface. The change in interfacial free energy when the dispersed droplet is deformed is then

$$\left(\frac{\partial G}{\partial A} \right)_{T,p,n} = \gamma + A \left(\frac{\partial \gamma}{\partial A} \right)_{T,p,n}, \quad (2)$$

assuming the number of surfactant molecules at the interface, n , is constant. This assumption is reasonable if the strain rate exceeds the inverse of the diffusion time for replenishment of the surfactant at the interface. The second-term, $\left(\frac{\partial \gamma}{\partial \ln A} \right)_{T,p,n}$, is known as the Gibbs elasticity and acts to enhance the resistance to deformation provided by the surface tension. The two terms are typically of the same order of magnitude. If the resistance to deformation exceeds the viscous stresses on the droplet then the droplet does not deform, the polymers experience little strain and the rheology of the fluid as it approaches pinch off is determined by the Newtonian character of the continuous phase. The ink can therefore be successfully printed.

Limiting the extent of deformation of the discontinuous phase during the printing process is of crucial importance for the principle to work. The deformation of a spherical droplet subjected to a straining flow in the continuous fluid was analyzed by Taylor.²³ Taylor solved the steady-state balance of forces on the deformed droplet; his model involves only the surface tension and not the Gibbs elasticity, which appears only in the time-dependent problem. Taylor's model therefore overestimates the deformation.

Taylor's theory is expressed in terms of the viscosity of the continuous phase, μ , the viscosity of the droplet, μ' , the undeformed radius of the droplet, r , the droplet interfacial tension, γ , and

the strain rate, σ . These parameters are grouped into the viscosity ratio, λ , and the capillary number, C , defined as

$$\lambda = \frac{\mu'}{\mu} \quad (3)$$

and

$$C = \frac{\sigma \mu r}{\gamma}. \quad (4)$$

Physically, the capillary number quantifies the relative magnitudes of viscous and interfacial forces. The drop deformation D can be expressed as

$$D = \frac{L - B}{L + B}, \quad (5)$$

where L is the half-length and B the half-breadth of the deformed droplet. In the limit of small deformations,

$$D = \frac{19\lambda + 16}{16\lambda + 16} C. \quad (6)$$

Thus, $D \approx C$ when $\lambda \gg 1$. Consequently, if we design an emulsion such that C is small under the high strain rates experienced in an ink jet, we would expect a droplet to maintain a spherical shape and thus prevent the coil-stretch transition that is the source of the difficulty in the ink-jet printing of high-MW polymers. Achieving this situation is not experimentally very difficult: for typical values of μ of $O(10^{-3} \text{ Pa s})$, γ of $O(10^{-2} \text{ N m}^{-1})$, r of $O(10^{-6} \text{ m})$ and σ of $O(10^5 \text{ s}^{-1})$, the capillary number is $O(10^{-2})$ and the extent of deformation is small. As noted above, on the very short timescales of ligament formation in an ink jet, the second term in Eq. (2) will act to reduce further the deformation.

For demonstration purposes, we formulated emulsions of $\sim 400 \text{ kDa}$ polystyrene (see below) as a $\sim 10\%$ wt solution in methyl benzoate dispersed in $\sim 15\text{-mM}$ sodium dodecylsulfate (SDS)

solution, with a dispersed phase fraction of 40 %wt. Single drops were jetted from a MicroFab print head (orifice diameter = 50 μm). The drop detachment process and the drying behavior on treated glass substrates were imaged with high-speed cameras. The uniformity of the deposits was investigated by interferometry.

EXPERIMENTAL

The polystyrene, PS, was kindly supplied by Dr L. Hutchings (Durham University, UK). Particulate material was removed by dissolving the PS in toluene, filtering the solution and recovering the PS through dropwise addition to methanol (Fisher, AR). Residual solvent was removed under vacuum at 70°C until the mass no longer changed. The PS was characterized by gel-phase chromatography (GPC) as having $M_n = 549$ kDa and polydispersity index, PDI = 1.06. GPC experiments were run on a Viscotek TDA 302 (Malvern) using samples of concentration 1 mg mL^{-1} in THF (Fisher, Chromatography GPC grade) and calibrated against linear polystyrene standards. Polymer solutions were prepared by dissolving the polystyrene in methyl benzoate (Acros Organics, 99%) and equilibration was ensured by gentle agitation overnight. The continuous phase of the emulsion was SDS (Sigma-Aldrich, >99.0%) dissolved in pure water (Milli-Q). The emulsion formulation comprised 9.5-%wt PS in methyl benzoate and a 14.8-mM SDS solution, with the discontinuous phase making up 40 %wt.

Rheological measurements were made on an AR 2000 (TA Instruments) using a cone-and-plate geometry; the cone had a 60 mm diameter. The emulsion had a constant viscosity of 5 ± 1 mPa s at strain rates 1 – 1000 s^{-1} . A 4%wt polystyrene solution had a constant viscosity of 45 ± 1 mPa s strain rates over the range 1 – 2000 s^{-1} .

The interfacial tension between the polymer and surfactant solutions was measured by pendant-drop tensiometry (First Ten Ångstroms, FTÅ200). Drops of 9.5-%wt PS in methyl benzoate (density $\rho = 1.082 \text{ g mL}^{-1}$) were suspended from a syringe in a cuvette filled with an 8.2-mM SDS solution ($\rho = 0.992 \text{ g mL}^{-1}$). Images were captured as silhouettes using a telescopic lens attached to a camera (Watec, Wat-902B) and were calibrated using a 3-mm sphere. The interfacial tension was extracted as 4.3 mN m^{-1} at 294 K using proprietary software (First Ten Ångstroms, Fta32 v2.0). The densities were measured using a 1.004-mL pycnometer at 294 K.

Emulsification of the formulation was achieved by briefly stirring the two components together to suspend the polymer solution in the continuous fluid, before applying an ultrasonic horn (Sonics, VC505) equipped with a 3-mm stepped microtip. The horn was operated at 25% amplitude for two minutes, followed by 40% amplitude for one minute. Sonication produces a polydisperse emulsion (Fig. 1a) comprising a small number of larger droplets with a radius of 1 – 6 μm and a much larger number of micron-sized droplets which together act to obscure the ordinarily black background. The largest droplets are an order of magnitude smaller than the print head orifice diameter (50 μm) so they should not perturb jetting. High-power ultrasound is known to lead to chain scission in polymers, so the polystyrene recovered from the emulsion was also characterized by GPC: the emulsified polymer had a reduced M_n of 419 kDa and an increased polydispersity of 1.21. We note that the presence of the polymer has a marked effect on the ultrasonic production of the emulsion: an emulsion generated in the absence of polystyrene under the same conditions (Fig. 1b) is far finer and more monodisperse, with a typical droplet radius of the order 1 μm . The polydispersity observed in Figure 1a is, therefore, due to the PS. The use of a homogenizer (IKA, T10 Ultra Turrax, $2 \times 10^4 \text{ rpm}$) in place of the ultrasonic horn did not improve the uniformity of the polymer-containing emulsions.

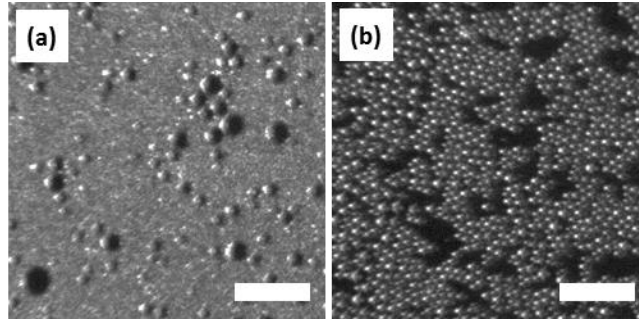


Figure 1. Dark-field images of emulsion aliquots sandwiched between two coverslips. (a) An emulsion of 9.5-%wt PS in methyl benzoate (40 %wt overall) and a 14.8-mM SDS solution. (b) An emulsion of methyl benzoate (40 %wt overall) and a 14.8-mM SDS solution; it has no polymer in the discontinuous phase. Images were captured using the printing rig, with illumination from LED 1 (see Fig. 2). The scale bars are 30 μm .

Figure 2 shows a schematic diagram of the rig used to print fluids and to visualize the jetting and drying processes. The fluid was contained in a reservoir and an overpressure was applied with a syringe. The reservoir was connected to the nozzle (MicroFab, MJ-ABP-01) by fluorinated ethylene propylene and silicone tubing (internal diameters 1.6 and 1 mm, respectively). The nozzle was actuated with a symmetrical bipolar waveform generated by the controller (MicroFab, JetDrive III Controller) and its amplitude was adjusted to ensure a single drop ($r \approx 35 \mu\text{m}$) was ejected each time. The drops were printed at $1 - 4 \text{ m s}^{-1}$, depending on the drive voltage, onto a hydrophobized glass substrate. Glass coverslips were washed with acetone and ethanol, placed in a bath sonicator in 2-%wt alkaline detergent solution (Decon Laboratories, Decon90) for 2 hours, rinsed in water (Milli-Q) and dried at $130 \text{ }^\circ\text{C}$ for 3 hours. Hexamethyldisilazane (Alfa Aesar, >98%) was deposited on the surface by vapor deposition in a

vacuum desiccator overnight. The coated substrates were rinsed in water and dried under an argon flow.

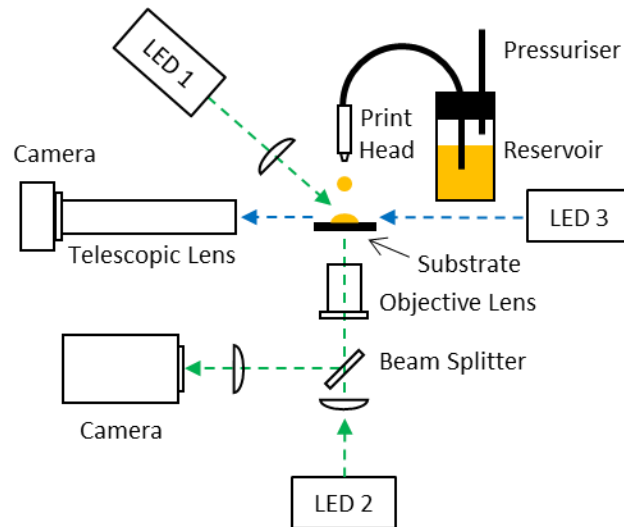


Figure 2. Schematic diagram of the rig used to print emulsion drops and image the drying process. Three LEDs were implemented to allow recording to take place on two high-speed cameras simultaneously from the side and from below. Unlabeled optics are plano-convex spherical lenses.

The printed drops were visualized simultaneously from below and from the side by high-speed cameras. To enable effective imaging of the drop on the substrate from beneath, two light sources were employed. The first was a collimated LED (Thorlabs, 505 nm, LED 1) mounted obliquely to the substrate with a lens condensing the light down to a focused spot. Interfaces within the printed drop scattered light, allowing the emulsion droplets to be visualized during the drying process. LED 1 did not adequately illuminate the large continuous structures that dominated towards the end of drying, particularly on the side of the printed drop furthest away from the light. A second source (Thorlabs, 505 nm, LED 2) was therefore mounted directly

below the drop and reflected by the upper surface of the substrate and the base of the printed drop. The light from these two LEDs was collected in the objective lens (Olympus, 50 \times , numerical aperture 0.5) mounted directly below and passed to the camera (Photron, FASTCAM APX RS). Images that show the side profile of the drop during drying were collected by another camera (Optronis, CR450x3) with a telescopic lens (LaVision, 12x Zoom Lens) and were illuminated by a collimated LED (Beaglehole Instruments, 455 nm, LED 3). A custom MATLAB routine was used to fit the profile to a spherical cap and thus determine evolution of the drop volume with time. In order to collect images of drop formation and detachment at the nozzle, a different high-speed camera (Photron, FASTCAM SA4) was used in place of the Optronis device. All images were calibrated using a slide featuring dots of a known size and spacing (LaVision, Micro Calibration Plate). Interferograms of deposits were recorded using a Talysurf CCI 6000 (Taylor Hobson).

RESULTS

The jetting dynamics of the emulsion are shown in Figure 3a. As fluid emerged from the nozzle, the drop necked under capillary pressure in keeping with its expected Newtonian character (Figs. 3a(i)–(iii)). Detachment took place at the orifice (Fig. 3a(iv)) and the remainder of the neck was drawn into the main drop body (Fig. 3a(v)). The speed of the drop after detachment was 1.1 m s⁻¹. The drop did not show the long-lived filament and elasticity commonly associated with printing polymer solutions, even though the overall concentration of polymer in the emulsion was 3.8 %wt. In contrast, Figure 3b shows how a 4.0-%wt PS solution in methyl benzoate behaved when printed. The PS implemented here had a slightly higher number-average molecular mass ($M_n = 549$ kDa) than the emulsion ($M_n = 419$ kDa) on account of the fact that it

had not been exposed to ultrasonic agitation. Attempts were made to print the polystyrene solution with a symmetrical bipolar waveform with drive voltages up to 100 V. Under no conditions was drop detachment observed. Instead, a column of fluid proceeded from the orifice (Figs. 3b(i)–(iii)), decelerated without any sign of necking, and was then drawn back inside the nozzle (Figs. 3b(iv)–(vi)).

The failure of the 4-%wt polymer solution to detach may lie in its high viscosity: the measured viscosity at low strain rates was 45 mPa s. The print head is rated for use with fluids of viscosity up to 20 mPa s, so the PS solution has physical properties outside the limits provided by the print head manufacturer. The PS solution may therefore be failing to detach on the basis of viscous dissipation of the fluid kinetic energy in the print head. The non-Newtonian properties of the solution are also likely to have an impact. The strain rates active in the ligament between the main drop body and the fluid in the orifice may be estimated using the images of the emulsion drop emerging from the print head. Between Figures 3a(ii) and 3a(iii), 17 μs has elapsed, but the radius of the ligament has approximately halved. For a cylinder of constant volume, a reduction in radius by factor of 2 must lead to an increase in length by a factor of 4. The extensional strain rate operational for a drop detaching from the print head is therefore $\sim 2 \times 10^5 \text{ s}^{-1}$. The Zimm relaxation time for a PS sample with mass-average molecular weight, $M_w = 488 \text{ kDa}$ in diethyl phthalate (DEP) has been reported as 84 μs .²⁴ The Zimm relaxation time $\tau_Z \propto \eta N^{3\nu}$, where μ is the solvent viscosity, N is the number of Kuhn monomers in the polymer and ν is the solvent quality.²⁵ At 298 K, the viscosity of DEP is 11 mPa s and the viscosity of methyl benzoate is 2 mPa s.²⁶ Taking both DEP and methyl benzoate to be good solvents ($\nu \sim 0.6$), for PS in dilute solution in methyl benzoate $\tau_Z \sim 20 \mu\text{s}$. The coil-stretch transition in dilute solution is thus expected at strain rates of approximately $2 \times 10^4 \text{ s}^{-1}$, an order of magnitude lower than the

typical strain rates operational during drop detachment in the print head. The 4 %wt PS solution is semi-dilute so the characteristic relaxation time estimated will be an overestimate, so that the coil-stretch transition is expected at even lower strain rates. The strain rates experienced by the 4 %wt PS solution are consistent with an elastic response. The failure of the 4 %wt PS solution to jet is likely a combination of both viscosity and elasticity. Nevertheless, the comparison of jetting dynamics for the polymer solution and the emulsion (Figs. 3a and 3b), which contained equivalent weight fractions of a high-MW polystyrene, shows that emulsions enable otherwise un-printable formulations to be jetted.

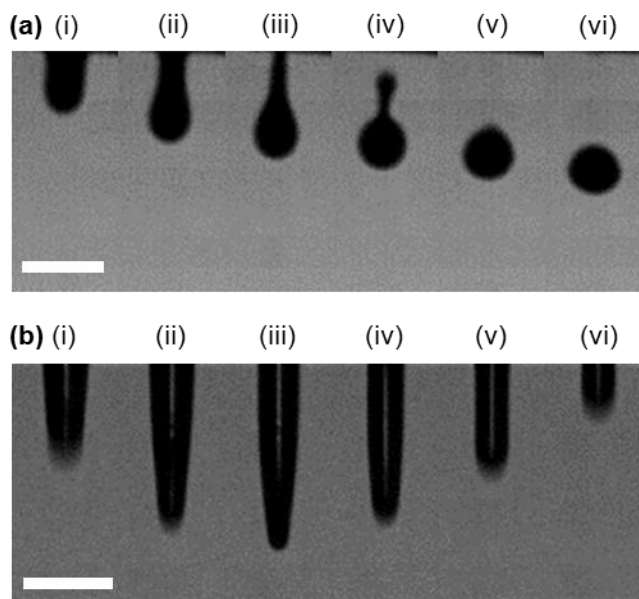


Figure 3. Jetting dynamics of various fluids driven by a symmetrical bipolar waveform and emerging from a 50- μm orifice. (a) An emulsion containing 3.8-%wt PS ($M_n = 419$ kDa) overall. The emulsion consisted of a 9.5-%wt methyl benzoate solution of PS (40 %wt overall) dispersed in a 14.8-mM SDS solution. The images were captured (i) 18, (ii) 36, (iii) 53, (iv) 71, (v) 89 and (vi) 107 μs after the fluid first emerged from the nozzle. The waveform was of amplitude 50 V. (b) A 4.0-%wt solution of PS ($M_n = 549$ kDa) in methyl benzoate, with images captured (i) 9, (ii)

18, (iii) 27, (iv) 36, (v) 44 and (vi) 53 μs after the fluid first emerged from the nozzle. The waveform was of amplitude 100 V. The scale bars are 100 μm .

The impact of using emulsions to print high-MW polymers was further investigated by printing PS solutions with a lower polymer content than 4 %wt. The timings of waveform used to actuate the print head was kept constant and the amplitude was varied to optimize jetting. A 2-%wt solution showed similar characteristics to those displayed in Figure 3b and detachment was not observed under any conditions. Detachment of drops from the orifice was observed for solutions of concentration 0.25, 0.50, 0.75 and 1.00 %wt, with drops speeds after detachment in the range 0.8 – 1.3 m s^{-1} . Figure 4 displays images of these solutions close to the point where the drop breaks off. Each formed long-lived filaments between the main drop body and the orifice; the length at detachment and the time of detachment increased with concentration. The non-Newtonian jetting dynamics are consistent with polymers undergoing the coil-stretch transition and introducing elasticity to the fluid, as discussed above. Additionally, the print head drive voltage required for detachment increased with concentration, from 15 V for 0.25 %wt PS to 53 V for 1.00 %wt PS. The characteristics of jetting for the 0.75 and 1.00 %wt solutions were poor, with the filament disintegrating into multiple satellites (Fig. 4c and 4d). The filament for the 0.50 %wt solution (Fig. 4b) led to the production of a single satellite that did not coalesce with the main droplet within 500 μm of the point of detachment. The 0.25 %wt solution detached comparatively quickly after emerging from the orifice (Fig. 4a) and produced a single satellite that coalesced when the main drop had travelled a further 35 μm . The 0.25 %wt PS solution has jetting characteristics the most like the emulsion (Fig 3a), but the emulsion contains 15 times

more polymer. The emulsion also did not show non-Newtonian jetting dynamics, which were observed for the 0.25 %wt solution (Fig. 4a). Emulsions thus provide a viable strategy for preventing polymers from undergoing the coil-stretch transition and causing disruptive non-Newtonian detachment dynamics.

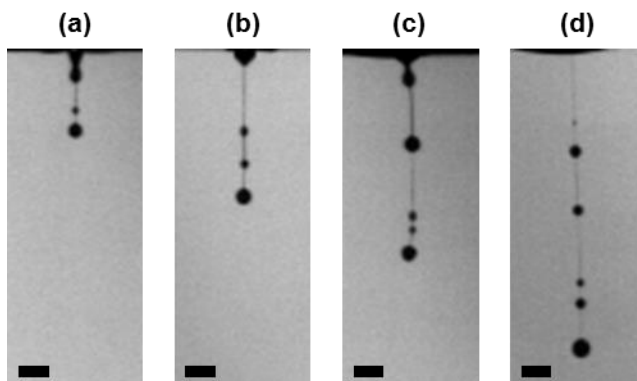


Figure 4. The effect of concentration upon the jetting behavior of solutions of PS ($M_n = 549$ kDa) in methyl benzoate. Fluids were jetted from a print head with a 50- μm orifice that was actuated with symmetrical bipolar waveforms. (a) A 0.25-%wt solution, captured 150 μs after the fluid first emerged from the nozzle. The waveform was of amplitude 15 V. (b) A 0.50-%wt, captured 200 μs after the fluid first emerged from the nozzle. The waveform was of amplitude 22 V. (c) A 0.75-%wt solution, captured 260 μs after the fluid first emerged from the nozzle. The waveform was of amplitude 27 V. (d) A 1.00-%wt, captured 370 μs after the fluid first emerged from the nozzle. The waveform was of amplitude 53 V. The scale bars are 100 μm .

Images of a drying emulsion drop of the same formulation as that used to determine drop detachment dynamics are shown in Figure 5a (imaged from below) and Figure 5b (imaged from the side). The total drying time was of the order 25 s. Evaporation of ink-jet printed drops are

known to be diffusion limited,²⁷ so the drying dynamics were controlled by the difference in vapor pressure and diffusion coefficient between the continuous and discontinuous phases. The reported vapor pressures, p_A , at 293 K are 2.3 kPa for water and 0.034 kPa for methyl benzoate.²⁶ The binary diffusion coefficients in air, D_A , for water and methyl benzoate are calculated as being 0.243 and 0.069 cm² s⁻¹, respectively, at 293 K using the empirical relationship recommended by Fuller²⁸ and corrected atomic/molecular diffusion volume increments for C, H and air.²⁹ The evaporation rate, r_A , for a component is proportional to $p_A D_A$ and, for water, to $p_A D_A (1 - RH)$, with the additional term taking into account the relative humidity, RH .³⁰ The predicted ratio of the evaporation rate of water to methyl benzoate at a typical RH of 0.4 is 140. There were, therefore, two distinct stages to the drying process: (1) rapid evaporation of the aqueous phase over the first 1.3 s after drop impact, with associated coalescence of the discontinuous phase into a single continuous oleic phase, and (2) slow evaporation of methyl benzoate over the subsequent 25 s.

Within 0.1 s of impact, the drop adopted a spherical cap with a diameter of about 130 μm (Figs. 5a(i) and 5b(i)). Initially the contents of the drop appeared bright, due to scattering from a large number of small oil droplets (Fig. 5a(i)). Larger droplets of dispersed phase were also visible as dark circles. Enhanced evaporation near the contact line induced convective transport of emulsion droplets towards the contact line (the so-called coffee-ring effect³¹) and an increased local concentration of oil droplets led to coalescence. At time $t = 0.3$ s, a continuous ring of polymer solution began to form at the contact line. Coalescence of the dispersed phase proceeded radially inwards (visible Figs. 5a(iii)–(v)) and the brightness of the drop reduced as more and more particles coalesced and there were fewer scattering centers (compare Figs. 5a(i)–(v)). A

continuous polymer solution remained once the aqueous phase had evaporated entirely: visually only a single phase remained after 1.3 s (Fig. 5a(vi)).

Figure 5b shows that the drop shape was a reasonable approximation to a spherical cap, with small deviations as the drop evolved from water-continuous to oil-continuous (Figs. 5b(iv)–(v)). The diameter and volume of the drop extracted from the footage is plotted against time in Figure 6. The diameter decreased by only 7 μm over the first 1.3 s, so that the loss of water was reflected in the decreasing height of the drop (Figs. 5b(i)–(v)) whilst the contact line remained largely pinned (Figs. 5a(i)–(v)). After complete evaporation of the aqueous phase, the remaining polymer solution adjusted its shape under surface tension and the contact line receded to reduce the diameter to 110 μm by $t = 1.8$ s (Figs. 5a(vii), 5b(vi) and 6), after which time the contact line stabilized. Evaporation continued to be reflected by decreasing drop height (Figs. 5b(vi)–(viii)) until a continuous PS deposit was left upon complete loss of solvent at $t = 24$ s (Fig. 5a(ix)).

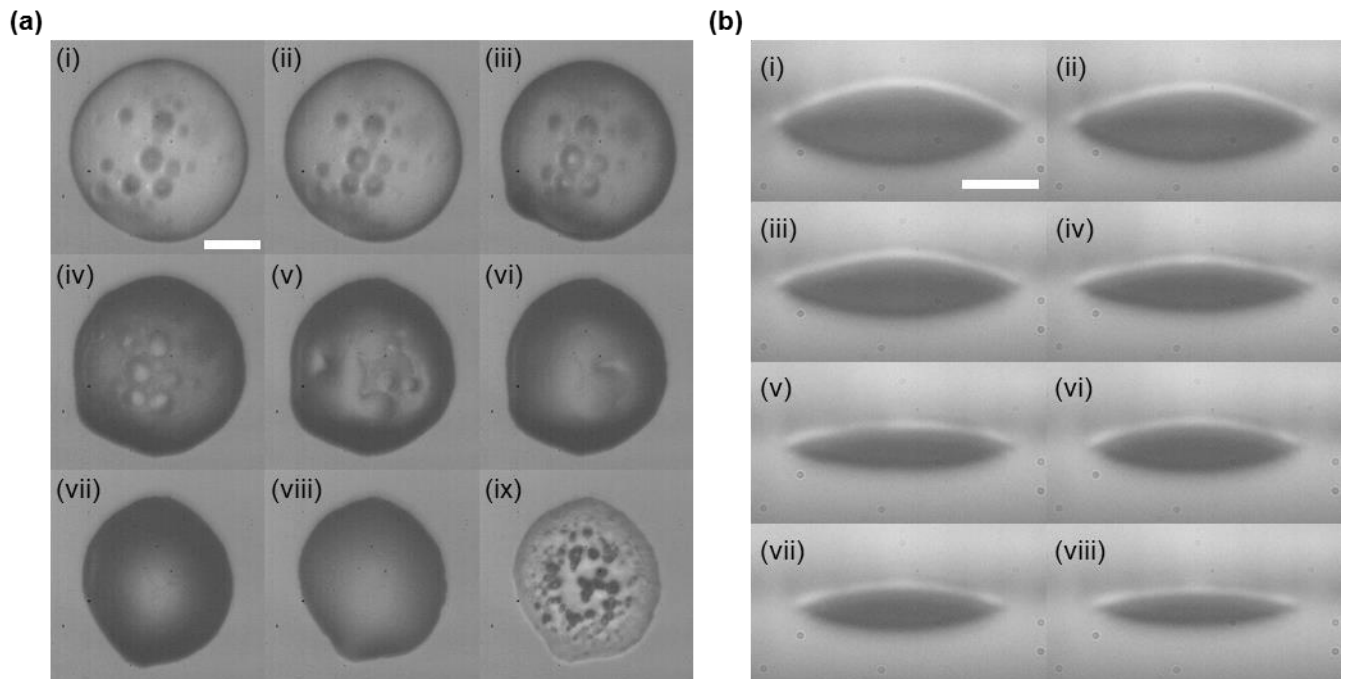


Figure 5. The drying process of an ink-jet printed drop of an emulsion containing polymer in the discontinuous phase. (a) The view from underneath, with images captured (i) 0.1 s, (ii) 0.3 s, (iii) 0.6 s, (iv) 0.9 s, (v) 1.2 s, (vi) 1.3 s, (vii) 1.8 s, (viii) 12.0 s and (ix) 24.0 s after the drop impacted the substrate. (b) The view from the side, with images captured (i) 0.1 s, (ii) 0.3 s, (iii) 0.6 s, (iv) 0.9 s, (v) 1.2 s, (vi) 1.8 s, (vii) 5.0 s and (viii) 10.0 s after drop impact. The emulsion consisted of a 9.5-%wt methyl benzoate solution of PS (40 %wt overall) dispersed in a 14.8-mM SDS solution. PS made up 3.8 %wt of the total formulation. The drop was ejected with a waveform amplitude of 100 V. The scale bars are 40 μm .

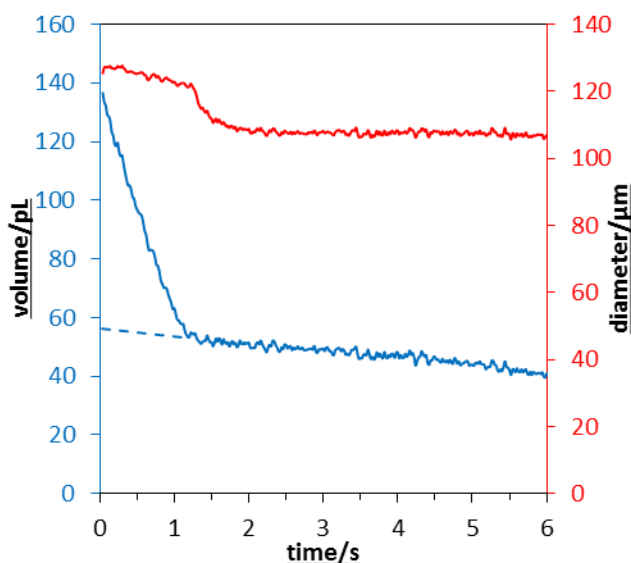


Figure 6. The volume change (blue solid line) and the diameter change (red line) of an ink-jet printed drop of an emulsion containing polymer in the discontinuous phase over the first six seconds of drying. This is the same drop as in Figures 5a and 5b. Volumes and diameters were determined by fitting a spherical cap to images of the drop obtained from the side. The initial volume of the discontinuous phase can be estimated by using linear regression to extrapolate the trend observed after 1.3 s back to time = 0 s (blue dashed line).

The rate of loss of volume was initially high at $74 \pm 7 \text{ pL s}^{-1}$, corresponding mainly to water evaporation (Fig. 6). At $t = 1.3 \text{ s}$ there was a sharp change in the rate of volume loss and evaporation proceeded at a much slower rate ($2.1 \pm 0.2 \text{ pL s}^{-1}$). The knee in the evaporation rate coincides approximately with the disappearance of two discrete phases in the images in Figure 5. After 1.3 s, only methyl benzoate remained and, as noted earlier, it had a much lower evaporation rate than water. The observed ratio of the rate of evaporation of water to that of methyl benzoate was 30, which is substantially lower than the expected ratio of 140.

If evaporation is diffusion controlled, then the rate of evaporation of methyl benzoate will depend only on the contact angle and drop diameter³⁰ and not on the presence of the aqueous phase. Hence, to estimate the initial volume of the oleic phase, the volume in Figure 6 at times greater than 1.3 s was extrapolated back to $t = 0 \text{ s}$, to yield a value of $55 \pm 5 \text{ pL}$. The initial drop volume was $140 \pm 10 \text{ pL}$. The volume fraction of the discontinuous phase was thus 41 %vol, or 45 %wt, and the overall PS concentration was 4.3 %wt, assuming that PS had a uniform concentration (9.5 %wt) across all dispersed phase species. The formulation was prepared with a discontinuous phase that comprised 40 %wt of the emulsion. The increase in the amount of discontinuous phase in the printed drop can be attributed to the tendency of the larger methyl benzoate droplets to sediment in water such that emulsified droplets collect at the nozzle. Thus in this single drop, the discontinuous phase had a proportion by weight about 12 % higher than the formulation average. In continuous printing applications, this segregation would not occur.

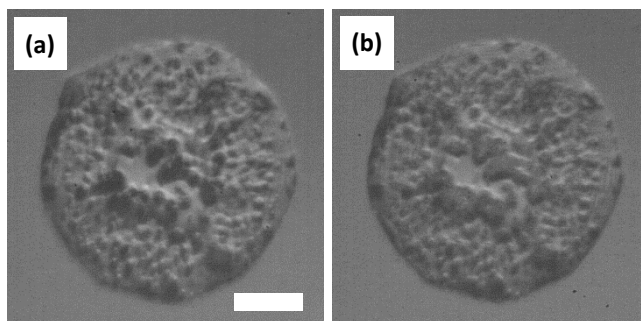


Figure 7. (a) An image of a dry polystyrene deposit left by a printed emulsion drop. (b) An image of the same deposit after it had been soaked in water for 30 min. The emulsion formulation was a 9.5-%wt methyl benzoate solution of PS (40 %wt overall) dispersed in a 14.8-mM SDS solution. PS made up 3.8 %wt of the total formulation. The drop was ejected with a waveform amplitude of 100 V. Images were captured using the printing rig, with illumination from LED 2 (see Fig. 2). The scale bar is 30 μm .

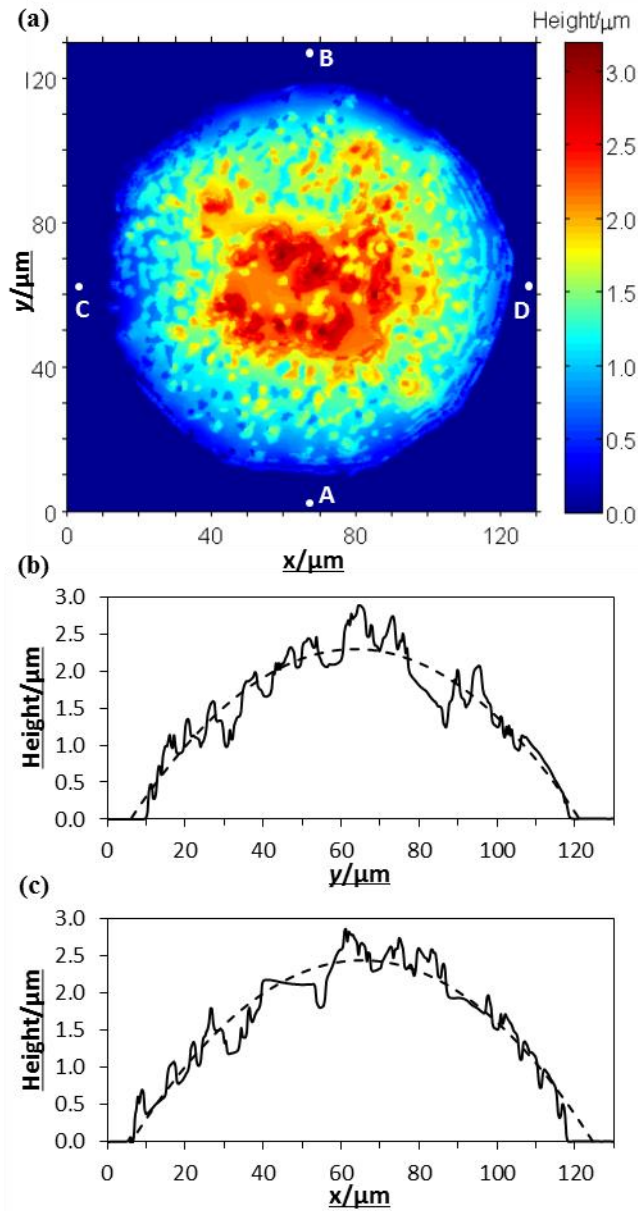


Figure 8. (a) A color map displaying the topography of the ink-jet printed emulsion drop in Figure 7a. The deposit surface was profiled using coherence correlation interferometry. (b), (c) The surface profiles along the vectors AB and CD respectively (solid lines) and the circular arc that best fit the data (dashed lines). Missing pixels in the interferogram were replaced by linear interpolation.

The polystyrene deposit (Fig. 5a(ix)) possessed a non-uniform distribution of features that are irregular in shape and appeared dark relative to the lighter colored, smoother surface surrounding them. The image of another dry deposit in Figure 7a shows even more pronounced irregularities. The illumination in the rig in Figure 2 is optimized to highlight interfaces in the evaporating drops and does not provide a quantitative measure of the irregularities in the surfaces. Consequently, we used interferometry to profile the height of the deposit in Figure 7a (see Fig. 8a). The deposit was dome shaped with a mean maximum height near the center of around 2.5 μm . Figures 8b and 8c represent orthogonal slices through the deposit and are overlaid by circular arcs fitted by a least-squares fitting routine. The circular arcs describe the overall cross sections well, with the fits characterized by standard deviations of 0.25 and 0.21 μm in Figures 8b and c respectively. The deposit can therefore be described as a spherical cap. The very large majority of the irregularities had lateral dimensions below 10 μm so that deviations from the smoothly varying arcs are in fact small and do not detract from the overall shape of the deposit. The deposit comprises both PS (~ 4 %wt in the initial formulation) and SDS (~ 0.25 %wt initially), since the latter is non-volatile. A possible origin of the surface irregularities in the dry deposits is the presence of SDS crystallized on the surface of the PS. Washing with water for 30 mins did not, however, change the image (Fig. 7b) so if the irregularities are due to residual surfactant then the surfactant must be buried within the polymer deposit. They may also arise from buckling of the polymer film in the later stages of drying.

DISCUSSION

Our jetting experiments show that we can print polymers at higher concentrations than is possible in solution. We were able to print an emulsion containing PS of $M_n = 419$ kDa at an

overall concentration of 3.8 %wt (Fig. 3a), but not a binary solution of the same concentration (Fig. 3b). We observed non-Newtonian jetting dynamics for PS solutions of concentration 0.50 – 1.00 %wt in the form of long-lived filaments that delayed drop breakoff and disintegrated into satellites. The PS solution that had the most comparable jetting dynamics to the emulsion was 0.25 %wt PS, which still formed a filament, but gave no satellites. A 0.25-%wt ink-jet printing limit has been observed elsewhere²¹ for jetting drops of a polystyrene ($M_n = 488$ kDa) solution in DEP at 6 m s^{-1} . We have therefore demonstrated that emulsions facilitate an improvement in the amount of polymer that can be delivered to a substrate in a single drop by an order of magnitude. This is advantageous for manufacturing scenarios since a layer of a certain thickness can be deposited in fewer passes, thus reducing process complexity. Our formulation also exhibited a two-stage drying regime which left a spherical cap of concentrated polymer solution after complete evaporation of the continuous phase. The resulting deposits were continuous and dome shaped: we did not observe ring stains commonly encountered for dispersed particulates.³¹ A uniform deposit is beneficial for most applications.

One disadvantage of the emulsion approach is the necessity to include a surfactant in the formulation, which may be undesirable for the functional properties of the deposited film. We experimented with a range of surfactants including well-known emulsifiers such as AOT and Tween80 as well as a cationic surfactant $C_{12}TAB$, but SDS gave the best emulsions. An SDS homologue with a lower cmc might permit a lower surfactant loading, but one will invariably need sufficient surfactant to form a substantial fraction of a monolayer at the oil-water interface; for micron-sized droplets a surfactant loading of less than 0.1 %wt is unlikely to be achieved. An alternative approach would be to use a lower molecular weight surfactant that is sufficiently

volatile to be removed during an annealing step, or possibly a photo- or thermally-degradable surfactant.

A challenge in using emulsions to print high-MW polymers is the manufacture of the emulsion itself. The ultrasonic preparation method leads to highly-polydisperse emulsions with small numbers of large droplets and large numbers of sub-micron droplets, which consume a lot of surfactant on account of their high collective surface area. The polydispersity has its origin in Ostwald ripening.³² PS is insoluble in water so it is unable to pass through the continuous phase under Ostwald ripening dynamics. The number of centers is then fixed, leading to a dispersity governed by Laplace pressure and polymer chemical potential. It is possible that a different processing procedure would yield better formulations. We tried low-shear emulsification methods, such as bath sonication and shaking by hand, to avoid polymer scission but found that emulsification was very poor. We deliberately kept the SDS concentration low (0.25 %wt) so that the major component of the deposit would be polystyrene.

The data in this paper represent the highest PS loading achieved. The polymer solution properties that inhibit printing also inhibit emulsification, since high strain rates are involved in the division of emulsified droplets. Increasing the polymer concentration in the fluid to be dispersed increases its non-Newtonian character and resulted in formulations with larger droplets of dispersed phase. Large droplets become problematic when they approach the size of the print head orifice since they impact jetting behavior. They are also not as effective at shielding polymers from high strain rates since deformation under shear is linear with radius, as in Eq. (6). The other way of increasing the polymer loading is to increase the volume fraction, ϕ , of the dispersed phase. The upper limit on ϕ is determined by the viscosity which is printable, which limits ϕ in practice to about 0.6.³³

A number of solvents were explored in developing the system described here. We have described these trials elsewhere³⁴ and just summarize the three main conclusions. (i) The dispersed phase should be a good solvent for the polymer in order to achieve a high polymer loading. (ii) The solvent should be significantly less volatile than water so that the drop evaporates in two discrete stages: first, evaporation of water and coalescence of the oleic phase into a uniform spherical cap and, second, evaporation of the organic solvent. However, the solvent should be sufficiently volatile that it dries within an acceptable processing time. For example, toluene ($p_A = 2.9$ kPa at 293 K) is too volatile and DEP ($p_A = 4 \times 10^{-5}$ kPa at 293 K) is too involatile.²⁶ (iii) Neutrally buoyant solvents such as anisole ($\rho = 0.995$ g mL⁻¹) give more uniform drop compositions than dispersed phases that cream (such as toluene, $\rho = 0.865$ g mL⁻¹) or sediment (such as DEP, $\rho = 1.12$ g mL⁻¹). Although methyl benzoate is denser than water, the density difference is small enough to allow successful printing but can lead, as shown in Figure 6, to droplets whose composition varies from the mean composition.

In principle, the same approach could be used to print water-soluble polymers in a water-in-oil emulsion. However, the continuous phase would need to be highly volatile (such as heptane) which may lead to difficulties with clogging of the ink-jet nozzles.

CONCLUSION

Oil-in-water emulsions provide a means for ink-jet printing high-MW polymers at a concentration much higher than is possible in a binary solution. The model formulation described in this paper comprised a 9.5-%wt polystyrene (PS: $M_n = 419$ kDa, PDI = 1.21) solution in methyl benzoate (40 %wt overall) dispersed in a 14.8-mM SDS solution. This emulsion could readily be jetted from a MicroFab nozzle (diameter 50 μ m) at 50 V to produce a single drop,

without any sign of the filaments and non-Newtonian behavior commonly associated with polymer solutions. In contrast, we were not able to print a binary solution in the same solvent with a similar overall concentration (~ 4 %wt) at any drive voltage, with emerging fluid always being drawn back into the nozzle. The emulsions function by shielding the polymer chains from extensional flow, which occurs solely in the continuous, aqueous medium. For typical jetting parameters and micron-sized droplets, capillary forces dominate viscous forces and the droplets of the dispersed phase, containing the polymer, remain close to spherical.

The drying of printed emulsion drops on a hydrophobized surface was observed with two high-speed cameras which capture images from underneath and from the side. We observed a two-stage drying process. Initially, drop behavior was dominated by water evaporation and emulsified droplets coalesced first at the contact line. Complete evaporation of the continuous phase left a spherical cap of the polymer dissolved in the organic solvent. A second, slower stage involved the evaporation of the organic solvent to leave a continuous deposit of the dry polymer. The PS deposits were profiled by interferometry and were found to have a dome shape with a central thickness of around $2.5 \mu\text{m}$ and a diameter around $110 \mu\text{m}$. Cross sections through the deposit showed a roughness with a standard deviation around one tenth of the height of the deposit. The topography may arise from embedding with the polymer deposit of crystals of the surfactant used to stabilize the emulsion, or from buckling of the polymer film in the later stages of drying.

The strengths of using emulsions to print high-MW polymer are that they allow an order-of-magnitude increase in the polymer loading compared to a binary solution and that they give a continuous deposit with approximately uniform coverage. We found, however, that the emulsification of the polymer solutions was not trivial and we were unable to generate

monodisperse emulsions. The viscoelastic characteristics of polymer solutions that inhibit jetting are also likely to hinder the breaking of larger drops into smaller ones. Involatile surfactants, such as SDS, used to stabilize the emulsion remain in the dry deposit, which may be undesirable for functional materials. Selection of solvents with appropriate volatility and density is important for printing of uniform polymer films.

AUTHOR INFORMATION

*Email: c.d.bain@durham.ac.uk

The manuscript was written through contributions of both authors. Both authors have given approval to the final version of the manuscript.

ACKNOWLEDGEMENTS

The authors are grateful to Dr. L. Yang for providing the MATLAB script used to extract volume and contact angle information from video files and to Mr. O. Burnham for assistance in carrying out GPC on polymer samples. We thank the Centre for Process Innovation for access to their interferometer. This work was funded by EPSRC under Grant EP/ H018913/1.

REFERENCES

- (1) Sweet, R. G. High Frequency Recording with Electrostatically Deflected Ink Jets. *Rev. Sci. Instrum.* **1965**, *36* (2), 131–136.
- (2) Zoltan, S. I. Pulsed Droplet Ejecting System. U.S. Patent 3,683,212, 1972.

- (3) Kyser, E. L.; Sears, S. B. Method and Apparatus for Recording with Writing Fluids and Drop Projection Means Therefor. U.S. Patent 3,946,398, 1976.
- (4) Basaran, O. A.; Gao, H.; Bhat, P. P. Nonstandard Inkjets. *Annu. Rev. Fluid Mech.* **2013**, *45*, 85–113.
- (5) *Inkjet Technology for Digital Fabrication*; Hutchings, I. M., Martin, G. D., Eds.; John Wiley & Sons, Ltd: Chichester, UK, 2013.
- (6) Mott, M.; Song, J.-H.; Evans, J. R. G. Microengineering of Ceramics by Direct Ink-Jet Printing. *J. Am. Ceram. Soc.* **1999**, *82* (7), 1653–1658.
- (7) Perelaer, J.; de Gans, B.-J.; Schubert, U. S. Ink-Jet Printing and Microwave Sintering of Conductive Silver Tracks. *Adv. Mater.* **2006**, *18* (16), 2101–2104.
- (8) Hoth, C. N.; Choulis, S. A.; Schilinsky, P.; Brabec, C. J. High Photovoltaic Performance of Inkjet Printed Polymer:Fullerene Blends. *Adv. Mater.* **2007**, *19* (22), 3973–3978.
- (9) Aernouts, T.; Aleksandrov, T.; Giroto, C.; Genoe, J.; Poortmans, J. Polymer Based Organic Solar Cells Using Ink-Jet Printed Active Layers. *Appl. Phys. Lett.* **2008**, *92* (3), 33306.
- (10) de Gans, B.-J.; Duineveld, P. C.; Schubert, U. S. Inkjet Printing of Polymers: State of the Art and Future Developments. *Adv. Mater.* **2004**, *16* (3), 203–213.
- (11) Sun, J.; Bao, B.; He, M.; Zhou, H.; Song, Y. Recent Advances in Controlling the Depositing Morphologies of Inkjet Droplets. *ACS Appl. Mater. Interfaces* **2015**, *7* (51), 28086–28099.

- (12) Spinelli, H. J. Polymeric Dispersants in Ink Jet Technology. *Adv. Mater.* **1998**, *10* (15), 1215–1218.
- (13) Christanti, Y.; Walker, L. M. Effect of Fluid Relaxation Time of Dilute Polymer Solutions on Jet Breakup Due to a Forced Disturbance. *J. Rheol.* **2002**, *46* (3), 733–748.
- (14) Xu, D.; Sanchez-Romaguera, V.; Barbosa, S.; Travis, W.; de Wit, J.; Swan, P.; Yeates, S. G. Inkjet Printing of Polymer Solutions and the Role of Chain Entanglement. *J. Mater. Chem.* **2007**, *17* (46), 4902–4907.
- (15) Amarouchene, Y.; Bonn, D.; Meunier, J.; Kellay, H. Inhibition of the Finite-Time Singularity during Droplet Fission of a Polymeric Fluid. *Phys. Rev. Lett.* **2001**, *86* (16), 3558–3561.
- (16) Entov, V. M.; Hinch, E. J. Effect of a Spectrum of Relaxation Times on the Capillary Thinning of a Filament of Elastic Liquid. *J. Nonnewton. Fluid Mech.* **1997**, *72* (1), 31–53.
- (17) Larson, R. G.; Magda, J. J. Coil-Stretch Transitions in Mixed Shear and Extensional Flows of Dilute Polymer Solutions. *Macromolecules* **1989**, *22* (7), 3004–3010.
- (18) Tirtaatmadja, V.; McKinley, G. H.; Cooper-White, J. J. Drop Formation and Breakup of Low Viscosity Elastic Fluids: Effects of Molecular Weight and Concentration. *Phys. Fluids* **2006**, *18* (4), 43101.
- (19) Christanti, Y.; Walker, L. M. Surface Tension Driven Jet Break Up of Strain-Hardening Polymer Solutions. *J. Nonnewton. Fluid Mech.* **2001**, *100* (1–3), 9–26.
- (20) de Gans, B.-J.; Kazancioglu, E.; Meyer, W.; Schubert, U. S. Ink-Jet Printing Polymers and Polymer Libraries Using Micropipettes. *Macromol. Rapid Commun.* **2004**, *25* (1), 292–

296.

- (21) Hoath, S. D.; Harlen, O. G.; Hutchings, I. M. Jetting Behavior of Polymer Solutions in Drop-on-Demand Inkjet Printing. *J. Rheol.* **2012**, *56* (5), 1109–1127.
- (22) van den Berg, A. M. J.; Smith, P. J.; Perelaer, J.; Schrof, W.; Koltzenburg, S.; Schubert, U. S. Inkjet Printing of Polyurethane Colloidal Suspensions. *Soft Matter* **2007**, *3* (2), 238–243.
- (23) Taylor, G. I. The Formation of Emulsions in Definable Fields of Flow. *Proc. R. Soc. A Math. Phys. Eng. Sci.* **1934**, *146* (858), 501–523.
- (24) Vadillo, D. C.; Mathues, W.; Clasen, C. Microsecond Relaxation Processes in Shear and Extensional Flows of Weakly Elastic Polymer Solutions. *Rheol. Acta* **2012**, *51* (8), 755–769.
- (25) Rubenstein, M.; Colby, R. H. *Polymer Physics*; Oxford University Press Inc.: New York, U.S.A., 2003.
- (26) *Chemical Properties Handbook: Physical, Thermodynamic, Environmental, Transport, Safety, and Health Related Properties for Organic and Inorganic Chemicals*; Yaws, C. L., Ed.; McGraw-Hill: New York, U.S.A., 1999.
- (27) Talbot, E. L.; Berson, A.; Brown, P. S.; Bain, C. D. Evaporation of Picoliter Droplets on Surfaces with a Range of Wettabilities and Thermal Conductivities. *Phys. Rev. E* **2012**, *85* (6), 61604.
- (28) Fuller, E. N.; Schettler, P. D.; Giddings, J. C. A New Method for Prediction of Binary Gas-Phase Diffusion Coefficients. *Ind. Eng. Chem.* **1966**, *58* (5), 18–27.

- (29) Fuller, E. N.; Ensley, K.; Giddings, J. C. Diffusion of Halogenated Hydrocarbons in Helium. The Effect of Structure on Collision Cross Sections. *J. Phys. Chem.* **1969**, *73* (11), 3679–3685.
- (30) Hu, H.; Larson, R. G. Evaporation of a Sessile Droplet on a Substrate. *J. Phys. Chem. B* **2002**, *106* (6), 1334–1344.
- (31) Deegan, R. D.; Bakajin, O.; Dupont, T. F.; Huber, G.; Nagel, S. R.; Witten, T. A. Capillary Flow as the Cause of Ring Stains from Dried Liquid Drops. *Nature* **1997**, *389* (6653), 827–829.
- (32) Kabal’nov, A. S.; Pertzov, A. V.; Shchukin, E. D. Ostwald Ripening in Two-Component Disperse Phase Systems: Application to Emulsion Stability. *Colloids and Surfaces* **1987**, *24* (1), 19–32.
- (33) Pal, R. Novel Viscosity Equations for Emulsions of Two Immiscible Liquids. *J. Rheol.* **2001**, *45* (2), 509–520.
- (34) Johns, A. S.; Bain, C. D. Using Emulsions to Overcome Problems Associated with the Inkjet Printing of High-Molecular-Weight Polymers in Solution. *NIP Digit. Fabr. Conf.* **2015**, *2015* (1), 476–480.

TOC GRAPHIC

